

Spike-Based Spatiotemporal Processing Enabled by Oscillation Neuron for Energy-Efficient Artificial Sensory Systems

Shuai Zhong, Yishu Zhang, Hao Zheng, Fangwen Yu, and Rong Zhao*

Developing an energy-efficient artificial sensory system is of great significance for neuroprosthesis, neurorobotics, and intelligent human-machine interfaces. Inspired by the biological perception, achieving this goal through spatiotemporal processing is viable. But some challenges, such as continuous signal coding resulting in high-energy consumption, are yet to be solved, hindering the realization of human perception emulation. Herein, a perceptual simulation enabled by spike-based spatiotemporal processing is demonstrated, which is analogous to the biological behavior, through an NbO_x -based oscillation neuron. The time difference between distinct inputs has a notable impact on the output spiking activity of oscillation neuron. On the basis of these features, the temporal-related perceptions, for example, direction selectivity and sound localization are closely imitated. Unambiguous differentiation of direction or azimuth is enabled according to the output spiking numbers of oscillation neuron. Furthermore, by combining the oscillation neuron with a spiking neural network, azimuth recognition is conceptually established to mimic the human's response to auditory stimuli. Herein, the feasibility of employing spike-based spatiotemporal processing of oscillation neurons to emulate sensory functionality, paving a highly potential way for realizing energy-efficient artificial sensory systems, is proved.

has implemented some sophisticated sensory functions. One elucidation for such characteristics of human sensory system is the spatiotemporal coding.^[9–15] Compared with the spatial-only coding, spatiotemporal coding involves an additional temporal dimension and enables a high density of information, thereby achieving higher energy efficiency.

Emulating the perception process of human is of great significance to the future neurorobotics, prosthetics, and human-machine interfaces.^[16,17] With the explosive growth of sensory data due to the advent of the information era and the rapid growth of Internet-of-Thing, it is imperative to develop artificial sensory systems that can process external information in an energy-efficient way. To achieve this goal, some attempts based on synaptic devices to emulate the perception via spatiotemporal processing have been made. For example, Wang et al. mimicked the orientation selectivity by obtaining the total excitatory postsynaptic current value

of Ag-based volatile memories.^[18] He et al. emulated the sound localization with a synaptic multiterminal neurotransistor. By comparing the difference between the output current triggered by the applied input voltage, azimuth could be distinguished.^[19] Despite these progresses, some challenges still remain. First, the continuous current coding generally leads to high energy consumption and heavy computational load. In fact, in biological sensory system, the spatiotemporal processing is carried out in the form of sparse, discrete spikes rather than continuous

1. Introduction

The human sensory system consisting of neurons and synapses allows to perceive the surroundings and react quickly to changes in the environment for survival.^[1–3] Environmental information is received by receptors and then transmitted to the brain/spine for processing via afferent nerves.^[4–6] This procedure is highly energy-efficient and much superior than the sensory systems built by current hardware and software,^[7,8] although the latter

S. Zhong, H. Zheng, F. Yu, R. Zhao
Department of Precision Instruments
Tsinghua University
Beijing 100084, China
E-mail: r_zhao@tsinghua.edu.cn

 The ORCID identification number(s) for the author(s) of this article can be found under <https://doi.org/10.1002/aisy.202200076>.

© 2022 The Authors. Advanced Intelligent Systems published by Wiley-VCH GmbH. This is an open access article under the terms of the Creative Commons Attribution License, which permits use, distribution and reproduction in any medium, provided the original work is properly cited.

DOI: 10.1002/aisy.202200076

Y. Zhang
ZJU-Hangzhou Global Scientific and Technological Innovation Center
College of Micro-Nano Electronics
Zhejiang University
Hangzhou 311200, China

R. Zhao
Innovation Center for Future Chip
Tsinghua University
Beijing 100084, China

R. Zhao
Center for Brain-Inspired Computing Research
Tsinghua University
Beijing 100084, China

signals.^[20,21] Second, the study on the spatiotemporal processing of neurons for sensory signals, which is supposed to be equally important as that of synapses, is limited, hindering the development of artificial sensory systems with high energy efficiency. Electrophysiological data has proved that neurons are the computational element for the spatiotemporal processing of spikes.^[13,22–24] Guided by these clues, implementing the spike-based spatiotemporal processing through neuronal computation may advance the development of energy-efficient sensory systems. Recently, the development of neuromorphic devices for artificial intelligence and edge computing has made great progress.^[25–27] Although not as widely studied as synaptic devices, artificial neuron has also attracted extensive attention and various devices have been successfully proposed to emulate the electrical dynamics of biological neurons. Among them, NbO_x- or VO_x-based Mott memristor is promising because of its insulator-to-metal transition and has been employed for applications such as fully memristive spiking neural network (SNN),^[28] central pattern generator network,^[29] and neural encoding for external stimuli.^[4,30,31] However, using it to mimic the spatiotemporal integration of biological neuron, especially for artificial sensory system, is quite limited.

Herein, we have realized spiking-based spatiotemporal processing for artificial perception by employing a NbO_x-based oscillation neuron. In particular, the direction selectivity and sound localization that are highly dependent on the temporal sequence of different inputs are well emulated. By examining the output spiking dynamics of the oscillation neuron, the direction or azimuth information carried by the input signals can be distinguished. We further demonstrate its feasibility of azimuth recognition task with the aid of an SNN algorithm. The output spikes of the neuron serve as the input of the SNN for training and recognition, achieving an accuracy of 96% of the sound position. This work proves the potential of spike-based spatiotemporal processing in realizing a bio-plausible, energy-efficient artificial sensory system.

2. Results and Discussion

A typical human visual system that processes external information in a spatiotemporal way for direction perception is illustrated in **Figure 1a**. Signals generated by car movement are first received by the receptor cells of the human eye, and then processed by retinal neurons called direction selectivity ganglion cells (DSGC),^[32] followed by transmission to the cerebral cortex. A detailed signal processing is presented in **Figure 1b**. The analog signals will be transduced to spike signals in the sensory receptor. These spikes travel along the afferent neural fibers to the DSGC through synaptic connections. In DSGC, all inputs with different timing are subtly integrated in the soma, and spikes carrying direction information are generated. Similar spatiotemporal processing can also be found in the human auditory system for sound localization, as shown in **Figure S1**, Supporting Information.

To emulate the sensory functionality driven by spatiotemporal processing, we design and fabricate an artificial neuron based on NbO_x memristor with a Pt/NbO_x/Pt structure. The electrical performance of the memristor is tailored by changing the pressure

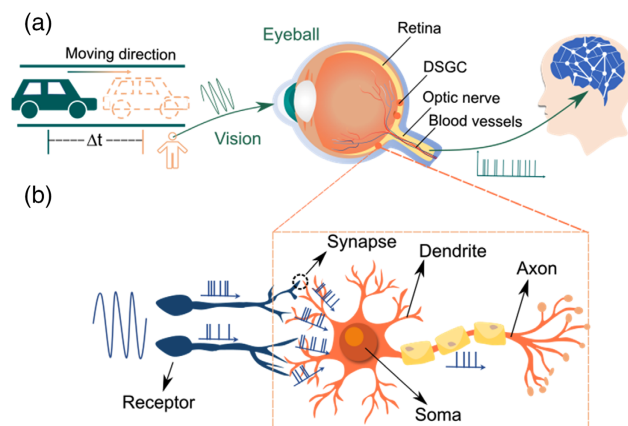


Figure 1. Schematic of the human visual system. a) An illustrative image of spatiotemporal processing of visual signal process. The signals produced by the moving car at different time will be integrated in the direction selectivity ganglion cells (DSGC) neuron for the spatiotemporal processing. b) Detailed working procedure of the spatiotemporal processing of DSGC neuron. The transduced spikes will transmit to the DSGC neurons that connect to the receptors via synapses. Through the spatiotemporal integration, spikes that represent the direction information are generated.

ratio of Ar and O₂ during the sputtering process to tune the oxygen stoichiometry of NbO_x (**Figure S2**, Supporting Information). The device with high switching uniformity is selected for the following study (Ar: O₂ = 19.25 : 0.75). **Figure S3**, Supporting Information, shows a schematic diagram of the device structure and the elemental characterizations, such as mapping and energy-dispersive spectra (EDS) line-scanning. The average atomic ratio of Nb:O is close to 2. **Figure 2a** depicts the DC electrical performance, which behaves a volatile threshold switching. The memristor switches from the high-resistance state (HRS) to the low-resistance state (LRS) when the applied voltage is larger than the threshold voltage (V_{th} , ± 2.2 V), and returns to the HRS if the applied voltage is lower than the holding voltage (V_{hold} , ± 1.8 V). The voltage distribution is demonstrated in **Figure 2b**. The coefficient of variation (CV) defined by the standard deviation (σ) and mean value (μ) is used to estimate the voltage uniformity. The CV values of $\pm V_{th}$, and $\pm V_{hold}$ are less than 0.5%, indicating excellent electrical reliability. Moreover, the device can be operated under different compliance currents, and a small device-to-device variation is observed (**Figure S4**, Supporting Information). Endurance performance is crucial for the memristor. A stable threshold switching is observed after 10^4 cycles, indicating reliable volatile property (**Figure S5**, Supporting Information). The resistive switching of NbO_x-based memristor can be ascribed to the well reported filament formation/rupture due to the trap-assisted conduction effect (**Figure S6**, Supporting Information), although other mechanisms such as Mott transition have also been suggested. Pulse performance is also studied by utilizing triangle voltages, as illustrated in **Figures 2c** and **S7**, Supporting Information. Repeatable transient switching in positive/negative sweeping is observed. The switch on and off speed is ≈ 60 ns at 2.3 V and ≈ 100 ns at 1.6 V, respectively, which is consistent with the V_{th} , V_{hold} in DC testing. Collectively, the results indicate that the NbO_x-based memristor has high reliability and fast switching speed.

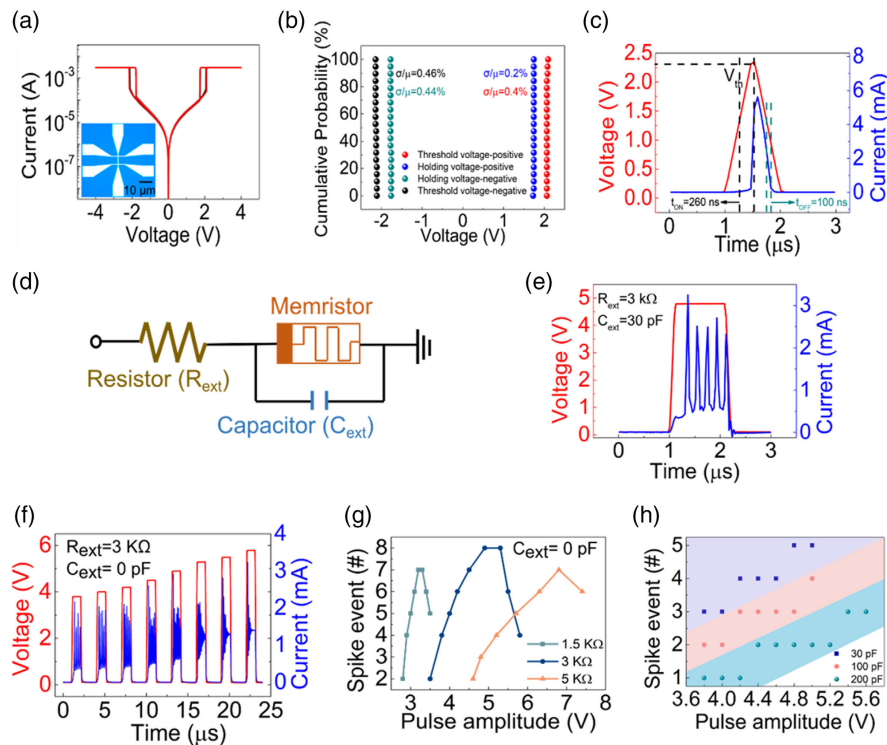


Figure 2. Electrical investigation of NbO_x-based memristor and artificial oscillation neuron. a) 20 cycles DC sweeping with the compliance current of 3 mA. Inset shows the optical image of memristor device. b) V_{th} and V_{hold} distribution of the memristor. The coefficient of variation (CV) for the positive V_{th} , V_{hold} and negative V_{th} , V_{hold} is 0.4%, 0.2% and 0.46%, 0.44%, respectively, indicating reliable volatile switching behavior. c) A triangle pulse with 2.4 V/1 μ s is employed to evaluate the switching speed. The speed for switching on and switching off is \approx 60 and 100 ns. d) The illustration of circuit implementation of an oscillation neuron based on NbO_x threshold switching memristor. A resistor is connected to the memristor in series and a capacitor connected to the memristor in parallel. e) The neural output of the oscillation neuron under the pulse (4.6 V/1 μ s) when a resistor of 3 k Ω and a capacitor of 30 pF were fixed. f) The effect of pulse amplitude on the spiking under the condition of $R_{ext} = 3$ k Ω and $C_{ext} = 0$ pF. g) Spiking dynamics of oscillation neuron connected to different resistors with no external capacitor (pulse width: 1 μ s). h) Spiking behavior when the memristor in parallel with various capacitors ($R_{ext} = 3$ k Ω).

By connecting the NbO_x-based memristor to a resistor (R_{ext}) in series and a capacitor (C_{ext}) in parallel (Figure 2d), an oscillatory neuron circuit is built. Generally, the resistance range of the R_{ext} is preferred between R_{HRS} and R_{LRS} ($R_{HRS} > R_{ext} > R_{LRS}$), while the C_{ext} can be the parasitic capacitance of the circuit ($C_{ext} = 0$ pF) or an external capacitor.^[33–35] At first, most of the applied voltage drops on the memristor since R_{HRS} is larger than R_{ext} , resulting in the charging of the capacitor. Once the voltage across the capacitor exceeds V_{th} , the memristor switches from the off-state to the on-state. Considering that R_{ext} is larger than R_{LRS} , the capacitor starts to discharge. Consequently, the memristor returns back to HRS when the voltage drops below V_{hold} . The repeatability of charging and discharging enables dynamic oscillation of the memristor. Figure 2e shows the typical oscillation behavior when R_{ext} and C_{ext} are fixed at 3 k Ω and 30 pF, respectively. A 1 μ s pulse can trigger the memristor to periodically switch between LRS and HRS. We further evaluate the oscillation through a cycling test and observe a reliable oscillation behavior after 250 pulses (Figure S8, Supporting Information).

To investigate how the input voltage intensity affects the output oscillatory spiking, a pulse train with gradually increasing amplitude is applied ($R_{ext} = 3$ k Ω , $C_{ext} = 0$ pF, Figure 2f). The number of generated spikes first increases as the pulse

amplitude increases, and then the oscillation becomes attenuated when the voltage exceeds a certain threshold. The possible cause of the damped spike is that the memristor remains in its “on” state. Furthermore, the relationship between R_{ext} and the spiking performance is also estimated, as displayed in Figure 2g. The voltage required to trigger the current spike increases as R_{ext} increases since more voltage will drop on the R_{ext} . The value of C_{ext} is another parameter to alter the spiking response of the oscillation neuron (Figure 2h). Evidently, for the same voltage, more spikes are produced when the memristor is connected in parallel with a smaller capacitor. This is because the charging time (t_{rise}) and the discharging time (t_{fall}) are proportional to the capacitor. Hence, a smaller capacitor provides a shorter t_{rise} and t_{fall} , contributing to more generated spikes. Specifically, if $R_{HRS} \gg R_{ext} \gg R_{LRS}$, the ideal spiking frequency f can be described by the following equation^[28,35]

$$f = \frac{1}{R_{ext} C \log\left(\frac{V_{hold} - V_{node}}{V_{th} - V_{node}}\right)} \quad (1)$$

where C includes the external capacitance (C_{ext}) and internal capacitance, while V_{node} is the applied voltage. We further estimate the average energy consumption of a single spike through

dividing the power consumption of the pulse by the number of spikes (Figure S9, Supporting Information). Energy consumption as low as ≈ 0.9 nJ per spike is achieved. It should be noted that this may vary with devices, and further improvement by device structure engineering is viable. The wide tunability of spike performance renders NbO_x -based memristors to mimic neuronal behavior for artificial sensory applications.

Using a NbO_x -based memristor, we build an oscillation neuron circuit that is similar to the biological neural circuit, as indicated in Figure 3a. The response of the oscillation neuron after the spatiotemporal integration of two different inputs with distinct timing differences is evaluated. If the excitatory and inhibitory incoming pulses arrive simultaneously, the neuron is silent and no spiking activity is detected (Figure 3b). When the excitatory input and inhibitory input arrive sequentially, neural spikes are perceived and the spiking frequency is largely associated with the temporal gap (see Figures 3c and S10, Supporting Information). Such spiking response governed by the time difference of inputs proves the spatiotemporal

processing of the oscillation neuron, which can be applied for emulations of perception.

Detecting the motion and direction of objects is an essential capability to help humans survive.^[36,37] The DSGC located in the retina is a specific neuron that accomplishes this task through complex spatiotemporal processing. Figure 3d sketches the working principle of direction selectivity. The photoreceptors (PR) receive the stimulus, transfer it to spiking signals, and pass them to the bipolar cells (BC). Once the signals from PR are collected, the BC produces excitatory spikes. Thereafter the generated spikes are delivered to the DSGC and starburst amacrine cells (SAC). It is worth noting that the excitatory input of SAC is converted to inhibitory output in dendrites.^[38,39] When a moving object is captured by the eyes, excitatory spikes and inhibitory spikes are generated successively, and then integrated in the DSGC to determine whether the neuron fires or the firing frequency. In the case of the object passing in a preferred direction, the excitation plays a dominating role, causing the neuron to fire strongly. In contrast, if the object moves in the null direction, the

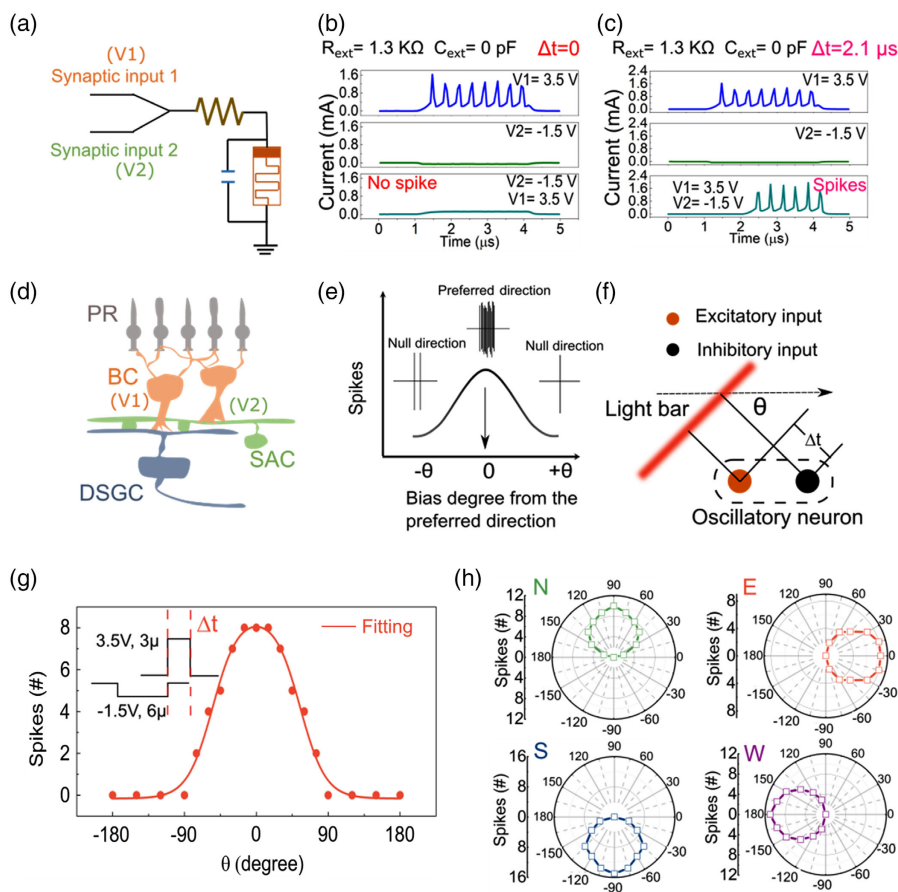


Figure 3. Spatiotemporal processing of oscillation neuron and its emulation of DSGC in visual sensory system for direction selectivity. a) The proposed circuit diagram of oscillation neuron for spatiotemporal integration. b) Current response when two inputs ($V1 = 3.5$ V, $V2 = -1.5$ V, pulse width = 3 μ s) were applied individually and simultaneously. c) Current response when two inputs ($V1$ and $V2$) were applied individually with a time interval (Δt) of 2.1 μ s. d) Schematic diagram of working principle of DSGC for direction selectivity. (PR: photoreceptor, BC: bipolar cells, SAC: starburst amacrine cells, DSGC: direction selectivity ganglion cells). e) Spiking response of DSGC to the moving object in different directions. Strong stimulus was triggered in the preferred direction while weak stimulus was observed in a null direction. f) Circumstance design to define the moving angle of light bar and time interval between excitatory input and inhibitory input. g) Spiking behavior of oscillation neuron as a function of the moving angle (time interval) in (f). Inset shows the details of two synaptic inputs. h) Polar plot of spikes represents four different directions (N: north, E: east, W: west, S: south).

inhibition “vetoes” the excitation, a shunting effect occurs and the neuron is prevented from responding, as demonstrated in Figure 3e. Previous inspiring work has been conducted to emulate the direction selectivity of DSGC through synapses with short-term memory. By investigating the total summation of postsynaptic currents resulted from spatiotemporal correlation of inputs, the direction selectivity can be achieved in a robust way. This is quite different from the situation in biological visual systems where spike frequency, rather than the amplitude of postsynaptic current, serves as the clue for the direction selectivity. A more bio-plausible approach is highly desired for the spike-based computation with high energy efficiency.

To simulate the DSGC spiking behavior in a biomimetic way, a scenario is carefully designed to determine the temporal relationship (Δt) between the excitatory and inhibitory inputs (Figure 3f). It can be easily found that Δt is highly dependent on the angle (θ) of the moving direction of the light bar. Thus, the moving direction can be calculated by analyzing the spiking response of the oscillatory neuron after spatiotemporal processing of inputs. Figure 3g exhibits the spiking trajectory when excitatory and inhibitory inputs with various timing gaps are applied to the oscillatory neuron under the condition described in Figure 3f. Here, we define that when the angle θ equals to zero, the time difference of inputs (Δt) is $3 \mu\text{s}$. In this case, the inhibitory pulse poses a negligible impact on the excitatory pulse, permitting the number of spikes of the oscillation neuron to reach its maximum. When the angle starts to increase clockwise/anticlockwise, the shunting effect emerges and hinders the neuron from firing. As a consequence, the spike number decreases and goes to 0 provided that the angle is greater than $90^\circ/-90^\circ$. Based on the dynamic change of the spike number, it is evident that the preferred direction of the oscillation neuron under this condition is East ($\theta = 0^\circ$). These results are in good agreement with the neural activity of DSGC when processing the external stimulus. It has been claimed that only four types of DSGCs in the retina and the preferred directions are classified as North (from bottom to top), South (from top to bottom), East (from left to right), West (from right to left).^[18] In addition to the DSGC with the preferred East direction, other types of DSGCs are also mimicked by the oscillation neuron in a similar manner (Figure S11, Supporting Information). Figure 3h displays the polar plots of the spike number of oscillation neurons as a function of θ under different situations, where the spike number is described by the radius of the circle. In this way, the geometries can visibly predict the preferred direction of four kinds of DSGC. The close resembling of direction selectivity in DSGC supports that spike-based spatiotemporal processing fulfilled by artificial neurons can mimic the biological sensory process in a bio-plausible way.

In addition to the direction selectivity, another critical perception related to spatiotemporal processing is sound localization,^[40,41] which is the ability to discern the relative orientation of a sound source. Recently, synapse-based sound localization was successfully realized by memristor or multiterminal oxide-based neurotransistor. By tracking the ratio of output voltages/currents caused by the inputs with different spatiotemporal relationships, the input sequence or the azimuth can be learned and recognized. Such demonstration undoubtedly advances the development of neuromorphic device to mimic

the spatiotemporal processing. While it also should be noted that in biological neural system, neurons are also the indispensable compartment that responsible for the spatiotemporal integration with spikes generated for the following processing. Thus, emulating spatiotemporal processing with neuronal device for perception is equally essential. For sound localization, the pivotal cue is the difference in arrival times of a sound between the two ears: interaural time difference (ITD).^[42] This cue extraction is done by neurons in the medial superior olive (MSO), which acts as coincidence detectors. It exhibits a relatively high spiking rate when the inputs of the two ears are synchronized ($\Delta t = 0$),^[43] or behind, there are few coincidences detected in MSO neurons ($\Delta t \neq 0$), resulting in a low spiking rate, as presented in Figure 4a. In the case where the sound is located near the contralateral ear (related to MSO neurons), the propagation time of the sound from the position to the MSO via contralateral ear may be equal to that via the ipsilateral ear ($\Delta t = 0$). Therefore, more coincidences in MSO neurons could be found, producing a high

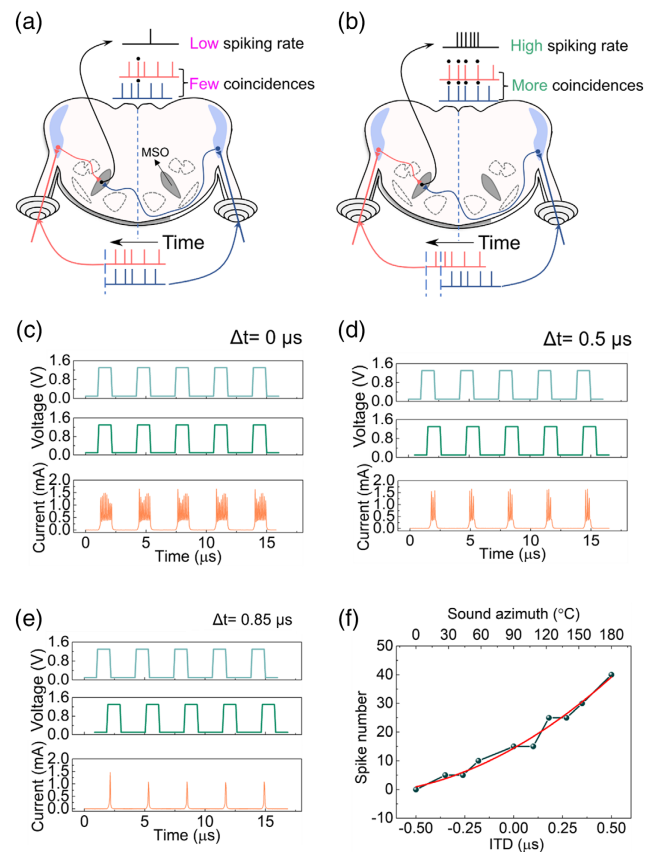


Figure 4. Emulation of the sound localization by oscillation neuron. a) Coincidence detection of medial superior olive (MSO) neuron when the interaural time difference (ITD) is 0. b) Coincidence detection of MSO neuron when the sound source locates close to the contralateral ear. Spiking response of oscillation neuron triggered by two identical pulse trains (1.3 V , $1 \mu\text{s}$ in pulse width, $2 \mu\text{s}$ in interval) with various time difference (ΔT): c) $\Delta T = 0 \mu\text{s}$, d) $\Delta T = 0.5 \mu\text{s}$, and e) $\Delta T = 0.85 \mu\text{s}$. f) Spiking dynamics of oscillation neuron changed with the ITD and the sound azimuth.

spiking rate. On the contrary, a sound source near the ipsilateral ear prevents the spiking of MSO neurons.^[44,45]

Such MSO neural behavior for sound localization can also be imitated by the spatiotemporal processing of oscillation neurons. Figure 4c presents the current spike response of the neuron when two identical synaptic inputs (1.3 V, 1 μ s in pulse width, 2 μ s in interval) are simultaneously delivered. The pulse synchronization successfully drives the neuron to fire, resulting in a spike frequency of about 2.67 MHz. When these two inputs are asynchronous with a time delay of 0.5 μ s, neuron firing is also monitored but the frequency is reduced to \approx 1 MHz, indicating that the mismatch tends to suppress the firing response (Figure 4d). This claim is confirmed by increasing the temporal delay of the pulse train to 0.85 μ s and using firing frequency of 0.33 MHz to alleviate the spiking activity of the oscillation neuron, as shown in Figure 4e. Not surprisingly, the neuron remains silent once the two synaptic inputs are completely staggered in time (Figure S12, Supporting Information). These results suggest that this oscillation neuron can serve as an indicator of pulse coincidence and can be used to simulate sound localization. To better emulate the performance of MSO neurons, we define that the time difference Δt is 0 if the sound source is positioned on the left (azimuth = 180°) and a larger value is assigned to Δt if the sound source stays on the right side (azimuth = 0°) on the basis of the aforementioned biological process (Figure 4b). The spike response as a function of the ITD and sound azimuth is shown in Figure 4f. The relative time of the inputs determines the activity of neural spiking, thus revealing cues to the sound location. The spiking number of neurons gradually increases proportionally to the sound azimuth, and their relationship can be fitted with an approximated linear curve, indicating that by examining the number of dynamic spikes, the location of the sound can be identified.

Reproducing the azimuth recognition is a key component of artificial sensory systems for human-machine interface and neurobotics to facilitate the interaction between the subjects and their surroundings. With this oscillation neuron, we replicated the process of azimuth recognition through applying an SNN algorithm. The spatiotemporal processed data related to sound localization is delivered to the SNN, as shown in Figure 5a. We perform cycles of pulse testing to create a dataset of sound azimuth. The data is split into two parts: 80% for the supervised training of the SNN and the remaining 20% for the testing. After 50 training epochs, the accuracy of sound direction recognition on the test data reaches 96% (see Figure 5b). Figure 5c,d shows the confusion matrices between the recognized direction and the input direction of training and testing, respectively. It is obvious that almost all direction signals can be well classified. Because of the high-accuracy output, we also conceptually perform the precise control of the steering angle of the robot based on the output spikes. As presented in Figure S13, Supporting Information, the synaptic inputs that represent the sound azimuth of 45° and 135° are processed by the artificial neuron and the SNN. Once receiving the inputs, the robot turns around 45° and 135°, accordingly. The successful demonstration of azimuth recognition signifies the great potential of the NbO_x-based oscillation neuron in the development of future artificial sensory systems.

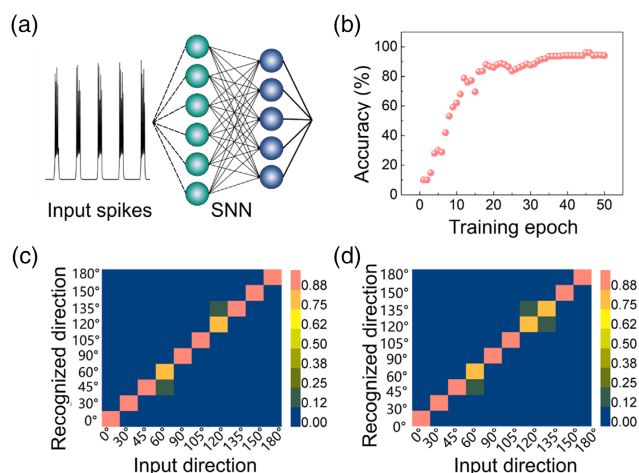


Figure 5. Implementation of azimuth recognition. a) Schematic of working processing that involves oscillation neuron and spiking neural network (SNN). b) Recognition accuracy of sound localization based on testing dataset. A high recognition rate of 96% was achieved after 50 training epochs. c) The confusion matrix between the input azimuth and the recognized azimuth for training dataset. d) The confusion matrix between the input azimuth and the recognized azimuth for testing dataset.

3. Conclusion

In summary, a spike-based spatiotemporal processing realized through oscillation neuron, which is analogous to the biological neuronal behavior in the human sensory system, is achieved for the energy-efficient artificial sensory systems by utilizing NbO_x threshold switching memristor. The spiking performance of artificial neuron shows rich adjustability and in particular, affected by the time difference of different inputs. Such characteristics allow it to imitate the perception functionalities that are highly associated with the spatiotemporal processing. For the demonstration, direction selectivity and sound localization are closely emulated. Moreover, combined with an artificial neural network, an artificial sensory system is accomplished to finish the azimuth recognition. The output of oscillation neuron after spatiotemporal processing are treated as the input to the neural network and a recognition accuracy of 96% is obtained. This work provides an inspiration for the future development of energy-efficient artificial sensory systems for neurobotics, prosthetics, and human-machine interfaces.

4. Experimental Section

Fabrication of NbO_x Volatile Memristor and Electrical Measurement: All the patterning was achieved by the photolithography and life-off process. First, 5 nm Ti was deposited on the Si/SiO₂ substrate as an adhesion layer. Then, 30 nm Pt layer bottom electrode was fabricated, followed by the deposition of NbO_x dielectric layer. NbO_x with different stoichiometries was obtained through controlling the Ar:O₂ ratio with a total gas pressure of 20 mTorr during the reactive sputtering. Finally, the Pt top electrode was sputtered with a thickness of 30 nm. All the electrical testing was performed using Agilent B1500A semiconductor parameter analyzer.

Materials Characterization: The sample was first prepared by focused ion beam (FIB) technique with a dual-beam system (Zeiss). Before that, a Pt protective layer was fabricated to avoid any damage during the cutting

treatment. Then, the sample was transferred to TEM system (Hitachi-S5500) for elemental analysis such as imaging, elemental mapping, and line scanning.

Training of Artificial Neural Network: The neural network shown in Figure 5a is two-layer fully connected SNN, with 25 input neurons and 10 output neurons. Spiking activation (leaky integrate-and-fire (LIF) neuron model) and a linear readout were used for first layer and last layer, respectively. For simplicity, the input data were normalized to the range from 0 to 1, and the connection weights used floating values. The training targets were that, for a sound direction, the corresponding output neuron should had an output value of 1, whereas other neurons had that of 0. All data falling to 10 directions were used for training. Mean squared error (MSE) was used to calculate the output loss function, and the loss function was backpropagated to preceding layers. Backpropagation through time (BPTT) was used to update the connection weights with a fixed learning rate of 0.02.

Setup of Robotic Vehicle Platform: The robotic system is based on a Clearpath Jackal robot. It contains a DAVIS 346 event camera, a Jetson Xavier NX computer, and a WHEELTEC Inertia Measurement Unit (IMU) N100. An Ubuntu 18.04 and a robotics operation system (ROS) Melodic were installed on the Jetson Xavier NX to process and control the car. The IMU was used to monitor the robotic current position and its movement.

Supporting Information

Supporting Information is available from the Wiley Online Library or from the author.

Acknowledgements

S.Z. and Y.Z contributed equally to this work. This work was supported by National Key R&D Program of China (No. 2018YFE0200200), National Nature Science Foundation of China (No. 61836004), Brain-Science Special Program of Beijing under grant Z181100001518006, The Suzhou-Tsinghua Innovation Leading Program (No. 2016SZ0102) and CETC Haikang Group-Brain Inspired Computing Joint Research Center.

Conflict of Interest

The authors declare no conflict of interest.

Data Availability Statement

The data that support the findings of this study are available from the corresponding author upon reasonable request.

Keywords

spike-based spatiotemporal process, artificial sensory systems, energy-efficient, oscillation neuron

Received: March 23, 2022
Revised: April 25, 2022
Published online: May 29, 2022

- [1] D. Li, K. Yao, Z. Gao, Y. Liu, X. Yu, *Light Adv. Manuf.* **2021**, 2, 1.
[2] M. Wang, Y. Luo, T. Wang, C. Wan, L. Pan, S. Pan, K. He, A. Neo, X. Chen, *Adv. Mater.* **2021**, 33, 1.
[3] X. Ji, X. Zhao, M. C. Tan, R. Zhao, *Adv. Intell. Syst.* **2020**, 2, 1900118.

- [4] X. Zhang, Y. Zhuo, Q. Luo, Z. Wu, R. Midya, Z. Wang, W. Song, R. Wang, N. K. Upadhyay, Y. Fang, F. Kiani, M. Rao, Y. Yang, Q. Xia, Q. Liu, M. Liu, J. J. Yang, *Nat. Commun.* **2020**, 11, 51.
[5] Y. Kim, A. Chortos, W. Xu, Y. Liu, J. Y. Oh, D. Son, J. Kang, A. M. Foudeh, C. Zhu, Y. Lee, S. Niu, J. Liu, R. Pfaffner, Z. Bao, T. W. Lee, *Science* **2018**, 360, 998.
[6] S. Chun, J. S. Kim, Y. Yoo, Y. Choi, S. J. Jung, D. Jang, G. Lee, K. I. Song, K. S. Nam, I. Youn, D. Son, C. Pang, Y. Jeong, H. Jung, Y. J. Kim, B. D. Choi, J. Kim, S. P. Kim, W. Park, S. Park, *Nat. Electron.* **2021**, 4, 429.
[7] M. Zeng, Y. He, C. Zhang, Q. Wan, *Front. Neurosci.* **2021**, 15, 1.
[8] S. Kim, D. G. Roe, Y. Y. Choi, H. Woo, J. Park, J. I. Lee, Y. Choi, S. B. Jo, M. S. Kang, Y. J. Song, S. Jeong, J. H. Cho, *Sci. Adv.* **2021**, 7, eabe3996.
[9] S. S. Radhakrishnan, A. Sebastian, A. Oberoi, S. Das, S. Das, *Nat. Commun.* **2021**, 12, 2143.
[10] Y. Li, J. Lu, D. Shang, Q. Liu, S. Wu, Z. Wu, X. Zhang, J. Yang, Z. Wang, H. Lv, M. Liu, *Adv. Mater.* **2020**, 32, 1.
[11] W. Wang, G. Pedretti, V. Milo, R. Carboni, A. Calderoni, N. Ramaswamy, A. S. Spinelli, D. Ielmini, *Sci. Adv.* **2018**, 4, 1.
[12] D. Saha, K. Leong, C. Li, S. Peterson, G. Siegel, B. Raman, *Nat. Neurosci.* **2013**, 16, 1830.
[13] R. Güti, H. Sompolinsky, *Nat. Neurosci.* **2006**, 9, 420.
[14] J. W. H. Schnupp, A. J. King, *Curr. Biol.* **2001**, 11, 640.
[15] A. V. M. Herz, T. Gollisch, C. K. Machens, D. Jaeger, *Science* **2006**, 314, 80.
[16] M. S. Kim, M. S. Kim, G. J. Lee, S. H. Sunwoo, S. Chang, Y. M. Song, D. H. Kim, *Adv. Mater. Technol.* **2021**, 7, 2100144.
[17] C. Wan, P. Cai, M. Wang, Y. Qian, W. Huang, X. Chen, *Adv. Mater.* **2020**, 32, 1.
[18] W. Wang, E. Covi, A. Milozzi, M. Farronato, S. Ricci, C. Sbandati, G. Pedretti, D. Ielmini, *Adv. Intell. Syst.* **2021**, 3, 2000224.
[19] Y. He, S. Nie, R. Liu, S. Jiang, Y. Shi, Q. Wan, *Adv. Mater.* **2019**, 31, 1.
[20] K. Roy, A. Jaiswal, P. Panda, *Nature* **2019**, 575, 607.
[21] J. Pei, L. Deng, S. Song, M. Zhao, Y. Zhang, S. Wu, G. Wang, Z. Zou, Z. Wu, W. He, F. Chen, N. Deng, S. Wu, Y. Wang, Y. Wu, Z. Yang, C. Ma, G. Li, W. Han, H. Li, H. Wu, R. Zhao, Y. Xie, L. Shi, *Nature* **2019**, 572, 106.
[22] A. J. Parker, W. T. Newsome, *Annu. Rev. Neurosci.* **1998**, 21, 227.
[23] C. Koch, *Nature* **1997**, 385, 207.
[24] N. Brunel, V. Hakim, M. J. E. Richardson, *Curr. Opin. Neurobiol.* **2014**, 25, 149.
[25] W. Wang, W. Song, P. Yao, Y. Li, J. V. Nostrand, Q. Qiu, D. Ielmini, J. J. Yang, *iScience* **2020**, 23, 101809.
[26] E. Covi, E. Donati, X. Liang, D. Kappel, H. Heidari, M. Payvand, W. Wang, *Front. Neurosci.* **2021**, 15, 611300.
[27] L. Sun, W. Wang, H. Yang, *Adv. Intell. Syst.* **2020**, 2, 1900167.
[28] Q. Duan, Z. Jing, X. Zou, Y. Wang, K. Yang, T. Zhang, S. Wu, R. Huang, Y. Yang, *Nat. Commun.* **2020**, 11, 3399.
[29] S. Dutta, A. Parihar, A. Khanna, J. Gomez, W. Chakraborty, M. Jerry, B. Grisafe, A. Raychowdhury, S. Datta, *Nat. Commun.* **2019**, 10, 3299.
[30] F. Li, R. Wang, C. Song, M. Zhao, H. Ren, S. Wang, K. Liang, D. Li, X. Ma, B. Zhu, H. Wang, Y. Hao, *ACS Nano* **2021**, 15, 16422.
[31] Q. Wu, B. Dang, C. Lu, G. Xu, G. Yang, J. Wang, X. Chuai, N. Lu, D. Geng, H. Wang, L. Li, *Nano Lett.* **2020**, 20, 8015.
[32] A. Borst, T. Euler, *Neuron* **2011**, 71, 974.
[33] P. Wang, A. I. Khan, S. Yu, *Appl. Phys. Lett.* **2020**, 116, 162108.
[34] S. K. Nandi, S. Li, X. Liu, R. G. Elliman, *Appl. Phys. Lett.* **2017**, 111, 202901.
[35] L. Gao, P. Y. Chen, S. Yu, *Appl. Phys. Lett.* **2017**, 111, 103503.
[36] D. I. Vaney, B. Sivyer, W. R. Taylor, *Nat. Rev. Neurosci.* **2012**, 13, 194.
[37] A. S. Mauss, A. Vlasits, A. Borst, M. Feller, *Annu. Rev. Neurosci.* **2017**, 40, 211.

- [38] A. W. Freeman, *J. Neurosci.* **2021**, *41*, 89.
- [39] D. I. Vaney, S. He, W. R. Taylor, W. R. Levick, *Direction-Selective Ganglion Cells in the Retina*, Springer, Berlin, Heidelberg **2001**.
- [40] J. C. Middlebrooks, *Handb. Clin. Neurol.* **2015**, *129*, 99.
- [41] G. Ashida, C. E. Carr, *Curr. Opin. Neurobiol.* **2011**, *21*, 745.
- [42] L. Sun, Y. Zhang, G. Hwang, J. Jiang, D. Kim, Y. A. Eshete, R. Zhao, H. Yang, *Nano Lett.* **2018**, *18*, 3229.
- [43] T. P. Franken, M. T. Roberts, L. Wei, N. L. Golding, P. X. Joris, *Nat. Neurosci.* **2015**, *18*, 444.
- [44] B. Grothe, M. Pecka, D. McAlpine, *Physiol. Rev.* **2010**, *90*, 983.
- [45] T. P. Franken, P. Bremen, P. X. Joris, *Front. Neural Circuits.* **2014**, *8*, 1.